TU Delft

Delft University of Technology

A Unified Thermal-Reactive Compositional Simulation Framework for Modeling CO_2 Sequestration at Various Scales

Wapperom, M.; Lyu, X.; Nichita, D. V.; Voskov, D.

DOI
10.2118/212182-MS

Publication date
2023

Document Version
Final published version

Published in
SPE Reservoir Simulation Conference 2023 Proceedings Papers

Citation (APA)
Wapperom, M., Lyu, X., Nichita, D. V., & Voskov, D. (2023). A Unified Thermal-Reactive Compositional Simulation Framework for Modeling CO_2 Sequestration at Various Scales. In *SPE Reservoir Simulation Conference 2023 Proceedings Papers* Article SPE-212182-MS (Society of Petroleum Engineers - SPE Reservoir Simulation Conference, RSC 2023). Society of Petroleum Engineers. https://doi.org/10.2118/212182-MS

Important note
To cite this publication, please use the final published version (if applicable).
Please check the document version above.

Copyright
Other than for strictly personal use, it is not permitted to download, forward or distribute the text or part of it, without the consent of the author(s) and/or copyright holder(s), unless the work is under an open content license such as Creative Commons.

Takedown policy
Please contact us and provide details if you believe this document breaches copyrights.
We will remove access to the work immediately and investigate your claim.

This work is downloaded from Delft University of Technology.
For technical reasons the number of authors shown on this cover page is limited to a maximum of 10.

Green Open Access added to TU Delft Institutional Repository

'You share, we take care!' - Taverne project

https://www.openaccess.nl/en/you-share-we-take-care

Otherwise as indicated in the copyright section: the publisher is the copyright holder of this work and the author uses the Dutch legislation to make this work public.

SPE-212182-MS

A Unified Thermal-Reactive Compositional Simulation Framework for Modeling CO_2 Sequestration at Various Scales

M. Wapperom, TU Delft; X. Lyu, China University of Petroleum Beijing; D. V. Nichita, University of Pau; D. Voskov, TU Delft, Stanford

Copyright 2023, Society of Petroleum Engineers DOI 10.2118/212182-MS

This paper was prepared for presentation at the SPE Reservoir Simulation Conference held in Galveston, Texas, USA, 28–30 March 2023.

This paper was selected for presentation by an SPE program committee following review of information contained in an abstract submitted by the author(s). Contents of the paper have not been reviewed by the Society of Petroleum Engineers and are subject to correction by the author(s). The material does not necessarily reflect any position of the Society of Petroleum Engineers, its officers, or members. Electronic reproduction, distribution, or storage of any part of this paper without the written consent of the Society of Petroleum Engineers is prohibited. Permission to reproduce in print is restricted to an abstract of not more than 300 words; illustrations may not be copied. The abstract must contain conspicuous acknowledgment of SPE copyright.

Abstract

In this work, we present a unified framework for the simulation of CO_2 sequestration problems at various time and space scales. The parametrization technique utilizes thermodynamic state-dependent operators expressing the governing equations for the thermal-compositional-reactive system to solve the nonlinear problem. This approach provides flexibility in the assembly of the Jacobian, which allows straightforward implementation of advanced thermodynamics. We validate our simulation framework through several simulation studies including complex physical phenomena relevant to CCUS. The proposed simulation framework is validated against a set of numerical and experimental benchmark tests, demonstrating the efficiency and accuracy of the modeling framework for CCUS-related subsurface applications. Important physical phenomena resulting from the complex thermodynamic interactions of CO_2 and impurities with reservoir fluids can be accurately captured now in detailed dynamic simulation. The investigated simulation scenarios include a reproduction of lab experiments at the core scale, investigation of macro-scale analog model and simulation of large-scale industrial application. The simulation time can also span from hours to years among various applications. Complex thermal-compositional-reactive phenomena can be addressed at each of these space and time scales. The unified thermodynamic description allows us to perform all these simulations for a reasonable CPU time due to advanced parametrization techniques and efficient GPU capabilities in our in-house reservoir simulator DARTS.

Keywords: CCUS, operator-based linearization, advanced thermodynamics, kinetics

Introduction

The development of methods for geological sequestration of CO_2 is of major importance towards realizing lower levels of atmospheric greenhouse gases. Permanent subsurface storage of CO_2 relies on a range of trapping mechanisms, which involve different physical aspects related to the characteristics of reservoirs and fluids. Structural trapping, analogous to the trapping of oil and gas, occurs when buoyant CO_2 is held in place by geological structures, overlain by a low permeable seal (Ajayi et al., 2019; Ringrose, 2020). In addition, the low permeability of the seal can create a capillary barrier to further invasion of the non-

Downloaded from http://onepetro.org/spersc/proceedings-pdf/23RSC/2-23RSC/D021S010R005/3095182/spe-212182-ms.pdf/1 by Bibliotheek TU Delft user on 18 April 2023

wetting CO_2. Other trapping mechanisms are less dependent on the geological features of a reservoir and include residual trapping, in which free gas CO_2 co-exists with brine and reservoir fluids but is trapped due to capillary forces, dissolution trapping in brine and mineral trapping, where CO_2 reacts with other chemical species to form solids (Pruess and Nordbotten, 2011; Fan et al., 2012; Delshad et al., 2013). The long-term security of storage is guarded by a combination of the above.

Suitable sedimentary formations for carbon sequestration include saline aquifers and depleted oil and gas fields, of which saline aquifers are most abundant in nature and hold the largest storage capacity. In assessing the potential, security and performance of such a reservoir for CO_2 storage, simulation models are used to predict fluids migration and chemistry, as well as pressure buildup and the geomechanical response within the reservoir. Given the uncertainties associated with subsurface characterization and the large number of ensembles needed for accurate modeling of subsurface processes, simulation models are required to consider the variety of physics at play and maintain robustness and efficiency. For this reason, a simulation framework must be able to capture the complex nature of the multiphase fluid systems, in addition to the advective-diffusive flow in the presence of gravity and capillary forces, in a robust and efficient manner.

The interaction between CO_2 and reservoir fluids may result in the occurrence of a range of fluid and solid phases, which may take place over different time scales. For example, upon injection of dry CO_2 into a brine saturated layer, the connate water slowly evaporates into the CO_2-stream. This can lead to an almost complete dry-out of the formation around the wellbore, possibly resulting in the precipitation of large amounts of solid salt, previously dissolved in the brine (Pruess and Müller, 2009; Kim et al., 2011). This effect is even more pronounced in heterogeneous rock due to capillary back-flow (Ott et al., 2015, 2021). Additionally, thermal effects related to injection of CO_2, such as Joule-Thomson cooling (Oldenburg, 2007), can complicate result in a temperature decrease that may even be sufficient to trigger the formation of hydrates.

In this work, we present a simulation framework that describes the physics related to thermal-compositional- reactive flow and transport in a unified manner. The presented framework is a modification of the existing Delft Advanced Research Terra Simulator (DARTS) platform (Khait and Voskov, 2018b; Lyu et al., 2021). It unifies the description of the conservation equations for mass and energy, with the addition of kinetic chemistry. DARTS uses the Operator-Based Linearization (OBL) technique for a generalized and efficient treatment of the different physical terms in the mass and energy balance equations (Voskov, 2016; Khait and Voskov, 2018a). This flexibility of the OBL approach allows straightforward implementation of advanced thermodynamics (Petitfrere et al., 2020). A generalized thermodynamic modelling framework is developed, in which a range of strategies for relevant fluid systems are highlighted.

A general description of phase equilibrium based on a combination of classic cubic equations of state for the CO_2-rich phase (Peng and Robinson, 1976) and an activity model for the aqueous phase (Ziabakhsh-Ganji and Kooi, 2012) is implemented. The activity model incorporates the effect of brine molality on phase behaviour, that translates into altered mutual solubilities of gases and water in the aqueous and the CO_2-rich phases, respectively. Equilibrium behaviour for ion and salt components is described by an activity product (Kala and Voskov, 2020). Accurate treatment of thermophysical properties enables the DARTS framework to capture important thermodynamic phenomena, such as the Joule-Thomson effect and the heat exchange upon reactions and phase changes.

We demonstrate that all-important physical phenomena can be effectively captured by the OBL approach. We use several existing numerical benchmarks to validate the accuracy of the developed framework in the dynamic representation of all these effects for modelling of CO_2 sequestration at various space and time scales.

Downloaded from http://onepetro.org/spersc/proceedings-pdf/23RSC/2-23RSC/D021S010R005/3095182/spe-212182-ms.pdf/1 by Bibliotheek TU Delft user on 18 April 2023

Simulation framework

In this section, we describe the governing equation and linearization approach for a unified thermal-reactive-compositional simulation framework utilized in this study.

Residual formulation of conservation equations

We assume that fluid flow is governed by advective-diffusive multiphase multicomponent formulation. The conservation equation for any species can be written as

$$\frac{\partial}{\partial t}\left(\phi\sum_{j=1}^{n_p}\rho_j s_j x_{cj}\right)+\nabla\cdot\left(\sum_{j=1}^{n_p}x_{cj}\rho_j\boldsymbol{u}_j+s_j\rho_j\mathbf{J}_{cj}\right)+\sum_{k=1}^{n_k}v_{ck}r_k=0\quad c=1,\ \ldots,\ n_c, \tag{1}$$

where ϕ is porosity, s_j is phase saturation, ρ_j is phase density [kmol/m^3] and x_{cj} is molar fraction of c component in j phase. Similarly, the energy conservation equation accounts for advective and conductive heat flow and contains contributions from both fluid and rock:

$$\frac{\partial}{\partial t}\left(\phi\sum_{j=1}^{n_p}\rho_j s_j U_j+(1-\phi)U_r\right)+\nabla\cdot\left(\sum_{j=1}^{n_p}h_j\rho_j\boldsymbol{u}_j+\kappa\nabla T\right)+\sum_{k=1}^{n_k}v_{ek}r_k=0. \tag{2}$$

Here U_j is phase specific energy [kJ/kmol] and U_r is rock specific energy [kJ/m^3] and κ is combined heat conduction term [kJ/day/K].

The velocity $\boldsymbol{u}_j$ follows the extension of Darcy's law for multiphase flow, which includes gravitational and capillary effects:

$$\boldsymbol{u}_j=\mathbf{K}\frac{k_{rj}}{\mu_j}\left(\nabla p_j-\boldsymbol{\gamma}_j\nabla z\right), \tag{3}$$

where $\mathbf{K}$ is the permeability tensor [mD], k_{rj} is the relative permeability of phase j, μ_j is the viscosity of phase j [mPa·s], p_j is the pressure of phase j [bars], $\boldsymbol{\gamma}_j=\rho_j\boldsymbol{g}$ is the specific weight [N/m^3] and z is the depth vector [m]. The diffusive flux $\mathbf{J}_{cj}$ of component c in phase j is described by Fick's law as

$$\mathbf{J}_{cj}=-\phi\,\mathbf{D}_{cj}\nabla x_{cj}, \tag{4}$$

where $\mathbf{D}_{cj}$ is the diffusion coefficient [m^2/day]. The source term related to kinetic reactions is a summation over the product of reaction rate r_k [kmol/m^3/day] and stoichiometry v_{ck}, or, if applicable, associated reaction heat v_{ek} [kJ/kmol], of each kinetic reaction k. The nonlinear equations are discretized using finite volume discretization with a two-point flux approximation and upstream weighting in space and a backward Euler approximation in time.

Operator form of conservation equations

The Operator-Based Linearization (OBL) approach simplifies the solution of discretized nonlinear system of equations (1) - (2) by introducing algebraic operators that capture all complex physics and nonlinear terms. Instead of keeping track of each property and its derivatives with respect to nonlinear unknowns, abstract algebraic operators representing the physics can be constructed and assembled into the set of Jacobian and residuals defined at each iteration. In the described approximation method, pressure, temperature and overall composition are taken as the unified state variables in a given control volume. The upstream weighting of the physical state is used to determine the flux-related fluid properties determined at the interface l. The discretized mass and energy conservation equation in operator form for each control volume will transfer to

$$V\phi_0\left[\alpha_c(\omega)-\alpha_c(\omega_n)\right]-\Delta t\sum_{l\in L(i)}\sum_{j=1}^{n_p}\left[\Gamma^l\beta_{cj}^l(\omega^\mu)\Delta\psi_j^l+\Gamma_d^l\gamma_j^l(\omega)\Delta\chi_{cj}\right]+\Delta tV\delta_c(\omega)=0,\quad c=1,\ \ldots,\ n_c, \tag{5}$$

Downloaded from http://onepetro.org/spersc/proceedings-pdf/23RSC/2-23RSC/D021S010R005/3095182/spe-212182-ms.pdf/1 by Bibliotheek TU Delft user on 18 April 2023

$$V\phi_0\left[\alpha_{ef}(\omega)-\alpha_{ef}(\omega_n)\right]-\Delta t\sum_{l\in L(i)}\sum_{j=1}^{np}\left[\Gamma^l\beta^l_{ej}(\omega^u)\Delta\psi^l_j+\Gamma^l_d\gamma_j(\omega)\Delta\chi_{ej}\right]+\Delta tV\delta_e(\omega)$$
$$+(1-\phi_0)VU_r\left[\alpha_{er}(\omega)-\alpha_{er}(\omega_n)\right]-\Delta t\sum_l(1-\phi_0)\Gamma^l_d\kappa_r\alpha_{er}(\omega)\Delta\chi_{er}=0, \quad (6)$$

where each operator represents a combination of physical properties and relations involved in the system (1) - (2).

In this form, most nonlinear parts of the system are defined only in terms of physical state-dependent functions. The values of these functions are uniquely determined in the parameter space of the simulation problem with the set of primary unknowns. Approximation interpolants are generated at each point in the discrete parameter space at the pre-processing stage and stored in $(n_c + 1)$-dimensional tables.

Thermodynamic modelling

In the reactive compositional formulation developed in this study, thermodynamic modelling is determining in accurate representation of the physics. Depending on the type of chemical species in the system and where one is located in the *PVT* -space, a variety of fluid and solid phases can co-exist. In this work, we consider saline aquifer conditions, which are limited to the occurence of saline aqueous solutions and a CO_2-rich phase, as well as the possibility of solid salt precipitation. Here, the principles of thermodynamic equilibrium will be reviewed and the procedures for flash and kinetic mechanisms will be presented.

Thermodynamic equilibrium

At thermodynamic equilibrium, pressure and temperature are uniform throughout the system. Furthermore, a necessary condition for equilibrium is that the chemical potential for each component is the same throughout all phases, or, equivalently, that the fugacities of the individual components are equal:

$$\hat{f}_i^j(T,P,\boldsymbol{n}_j)=\hat{f}_i^k(T,P,\boldsymbol{n}_k),\quad i=1,\ \ldots,n_c \quad (7)$$

between all phases j and k. Finally, the system is at equilibrium if and only if the total Gibbs energy is at its global minimum. This requires finding the conditions at which the Gibbs energy is at a minimum for all possible combinations of phases. The Gibbs free energy is given by:

$$G^*=G/RT=\sum_{j=1}^{n_p}\sum_{i=1}^{n_c}n_{ij}\ln\hat{f}_{ij} \quad (8)$$

with n_{ij} the number of moles of species i in phase j.

A material balance for each component yields

$$x_{i0}+\sum_{j=1}^{n_p-1}\nu_j(x_{ij}-x_{i0})=z_i,\quad i=1,\ \ldots,n_c \quad (9)$$

with phase 0 the reference phase. Finally, mole fractions in the different phases must sum to unity, yielding

$$\sum_{i=1}^{n_c}(x_{ij}-x_{i0})=0,\quad j=1,\ \ldots,n_p-1 \quad (10)$$

For two phases, the system to be solved amounts to n_c material balances, n_c equilibrium equations and one summation of mole fractions constraint, yielding $2n_c + 1$ relations between the $2n_c + 3$ unknowns, T,P, $\boldsymbol{x}$, $\boldsymbol{y}$, ν_1, where pressure and temperature are specified for a *PT* -flash.

Downloaded from http://onepetro.org/spersc/proceedings-pdf/23RSC/2-23RSC/D021S010R005/3095182/spe-212182-ms.pdf/1 by Bibliotheek TU Delft user on 18 April 2023

Solution methods for equilibrium calculations

Phase equilibrium calculations are concerned with finding the amount and composition of the different equilibrium phases present. The aim is to satisfy the material balance and equifugacity constraints. Following Michelsen and Mollerup (2007), the equilibrium equations are written as:

$$\ln y_i - \ln x_i = \ln K_{il} = \ln \varphi_i^j - \ln \varphi_i^k, \quad l = 1, \ldots, n_p - 1 \tag{11}$$

The solution procedure must be initiated with an initial guess of the set of K-values, after which fugacity coefficients can be updated. Often, this procedure involves a number of iterations of successive substitution. Here, the material balance is satisfied by solving the Rachford-Rice equations in an inner loop, in which the fugacity coefficients are assumed composition-independent, and fugacities are updated in an outer loop. The Rachford-Rice equation for an arbitrary number of phases can be obtained by introducing equilibrium constants K_{ij} and substituting the phase compositions from (9) into the mole fraction relation (10), written as:

$$R_j = \sum_{i=1}^{n_c} \frac{z_i\left(K_{ij} - 1\right)}{1 + \sum_{l=1}^{n_p - 1} \nu_l\left(K_{il} - 1\right)} = 0, \quad j = 1, \ldots, n_p - 1 \tag{12}$$

For two phases, equation (12) represents a monotonically decreasing function within the negative flash window, that is, the region characterized by all non-negative phase compositions. A non-trivial solution with a negative phase fraction – either $v < 0$ or $v > 1$ - indicates stability of the feed with the same certainty as a stability test (Whitson and Michelsen, 1989). In our work, the Rachford-Rice equation is solved using convex transformations, as proposed by Nichita and Leibovici (2013), leading to a significant increase in solution speed.

Under typical saline aquifer conditions, the chemical species of interest that occur in fluid phases include CO_2, H_2O, ions and possibly impurities in the CO_2-stream, typically gases and light hydrocarbons. These split among the brine and the non-aqueous CO_2-rich phases. For the phase equilibrium calculations presented in this work, an activity model is used to model the aqueous phase (Ziabakhsh-Ganji and Kooi, 2012), which incorporates the effect of brine salinity on solubilities, and the PR equation of state (Peng and Robinson, 1976) represents the non-aqueous phases.

Kinetics

In thermodynamic calculations for a system in which chemical reactions occur, additional degrees of freedom are available. As the system is away from equilibrium, it continuously attempts to reach chemical equilibrium by an exchange of matter between phases through chemical reactions, driven by the difference in chemical potential. At thermodynamic and chemical equilibrium, the system has reached its condition of maximum thermodynamic stability and there is no potential to alter the mass distribution among the phases.

The equilibrium behaviour of a reversible chemical reaction is often described by the law of mass action (Kala and Voskov, 2020). For a chemical reaction

$$p\,\mathrm{A} + q\,\mathrm{B} \rightleftharpoons r\mathrm{C} + s\mathrm{D} \tag{13}$$

the activity product is given as

$$Q = \frac{[\mathrm{C}]^r[\mathrm{D}]^s}{[\mathrm{A}]^p[\mathrm{B}]^q} \tag{14}$$

The assumption of instantaneous equilibrium as stated for the multiphase flash calculations cannot always be used in chemically reacting systems. Equilibrium in such systems is governed by the competition between the reaction and the transport processes. If the reactive processes are faster in relation to transport of species, local equilibrium is a reasonable assumption. If not, the dynamics of such reactions must be described using a kinetic mechanism. The rate at which kinetic reactions that follow (14) take place is generally expressed as:

Downloaded from http://onepetro.org/spersc/proceedings-pdf/23RSC/2-23RSC/D021S010R005/3095182/spe-212182-ms.pdf/1 by Bibliotheek TU Delft user on 18 April 2023

$$r_k = c_k A\left(1 - \Omega^p\right)^q \tag{15}$$

where c_k is a reaction constant and A is the reacting surface area. The kinetic saturation state reads $\Omega = Q/K^{eq}$, where K^{eq} is the equilibrium product. The sign of $(1 - \Omega)$ determines the deviation from equilibrium. In this work, we use this kinetic model for the precipitation and dissolution of sodium chloride from brine:

$$Na^+(aq) + Cl^-(aq) \rightleftharpoons NaCl(s) \tag{16}$$

Results

In this section, we show an application of the developed framework to problems relevant to CO_2 sequestration. We start with the prediction of thermodynamic parameters and follow up with integrated simulations involving various phenomena relevant to CCUS.

Thermodynamic properties for CCUS-related applications

In the thermal-compositional simulation framework, accurate modelling of thermodynamic properties is important to capture the different trapping mechanisms for CO_2. In this section, we present fluid properties over a range of pressure and temperature relevant to CCUS and discuss the implicated physical phenomena.

Figure 1 presents the mutual solubilities of CO_2 and H_2O. For the simulation model to accurately represent each of the primary trapping mechanisms, these properties are of critical importance. The phase compositions determine phase density and viscosity, governing the migration path of the CO_2-rich plume. Furthermore, the density of the gas will influence the height of a gas cap trapped by a capillary barrier. In relation to dissolution trapping, the solubility of CO_2 in water and the increased density of CO_2-saturated brine create gravity-induced currents that result in a fingering pattern, which is the main driver behind dissolution trapped CO_2.

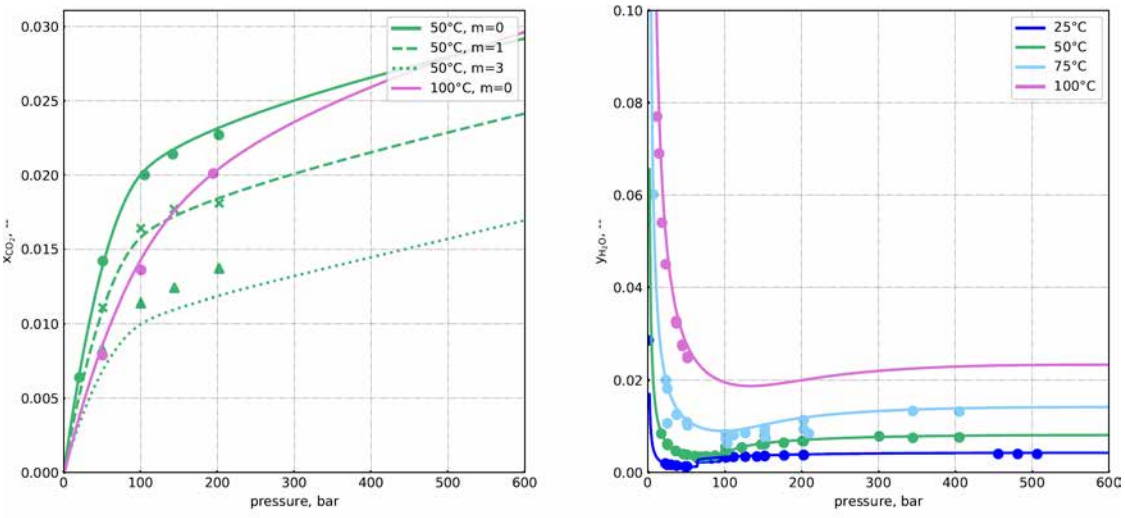

(a) CO_2 in aqueous phase (b) H_2O in CO_2-phase

Figure 1—Mutual solubilities of CO_2 and H_2O. (a) Solubility of CO_2 in the aqueous phase, data from (Koschel et al., 2006), and (d) solubility of H_2O in the CO_2-phase, data from (Spycher et al., 2003)

On the other hand, the solubility of H_2O in the CO_2-rich phase is a factor in drying out of the near-wellbore region. Although the solubility is low, continuous evaporation of brine into the dry CO_2 injection stream, together with capillary effects could eventually result in an accumulation of solid salt that causes significant reductions in well injectivity.

Downloaded from http://onepetro.org/spersc/proceedings-pdf/23RSC/2-23RSC/D021S010R005/3095182/spe-212182-ms.pdf/1 by Bibliotheek TU Delft user on 18 April 2023

In our formulation of the conservation of energy (2), enthalpy changes related to the Joule-Thomson effect, as well as dissolution, evaporation, phase changes and reactions are included implicitly through the consistent treatment of enthalpy. This implies a range of thermophysical phenomena associated with CO_2 injection.

The Joule-Thomson effect is referred to as the temperature change that accompanies a pressure drop in a real gas or liquid, in the absence of heat exchange with the surroundings (at constant enthalpy, i.e., adiabatic expansion), and can occur upon the injection and expansion of CO_2 into the lower pressured surroundings of a well. The temperature change accompanied by a pressure change is defined by the Joule-Thomson coefficient

$$\frac{\Delta T}{\Delta P} \approx \left(\frac{\partial T}{\partial P}\right)_H = \mu_{JT} \tag{17}$$

For most common gases at conditions of interest, μJT is positive, and consequently the temperature drops with a pressure drop. Figure 2 shows the Joule-Thomson coefficient of pure CO_2 and various mixtures of CO_2-CH_4. The temperature drop is most pronounced for systems under subcritical conditions.

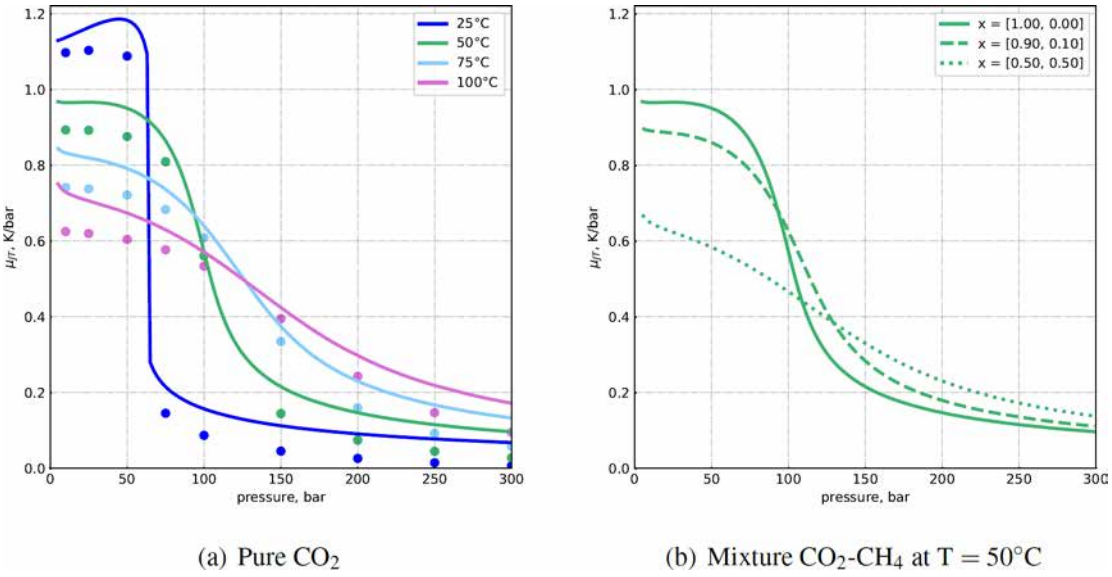

(a) Pure CO_2 (b) Mixture CO_2-CH_4 at T = 50°C

Figure 2—Joule-Thomson coefficient for (a) pure CO_2, data from (Lemmon et al., 2022), and (b) mixture of CO_2-CH_4

In addition, conditions may be such that a pressure drop is associated with a phase change from liquid CO_2 to gaseous, the enthalpy of vaporization that is required for this phase change further cools down the surroundings. Additionally, there is an enthalpy change associated with mixing between brine and CO_2. In Figure 3, the enthalpy of pure CO_2 and the enthalpy change of CO_2 dissolution into brine are displayed.

Downloaded from http://onepetro.org/spersc/proceedings-pdf/23RSC/2-23RSC/D021S010R005/3095182/spe-212182-ms.pdf/1 by Bibliotheek TU Delft user on 18 April 2023

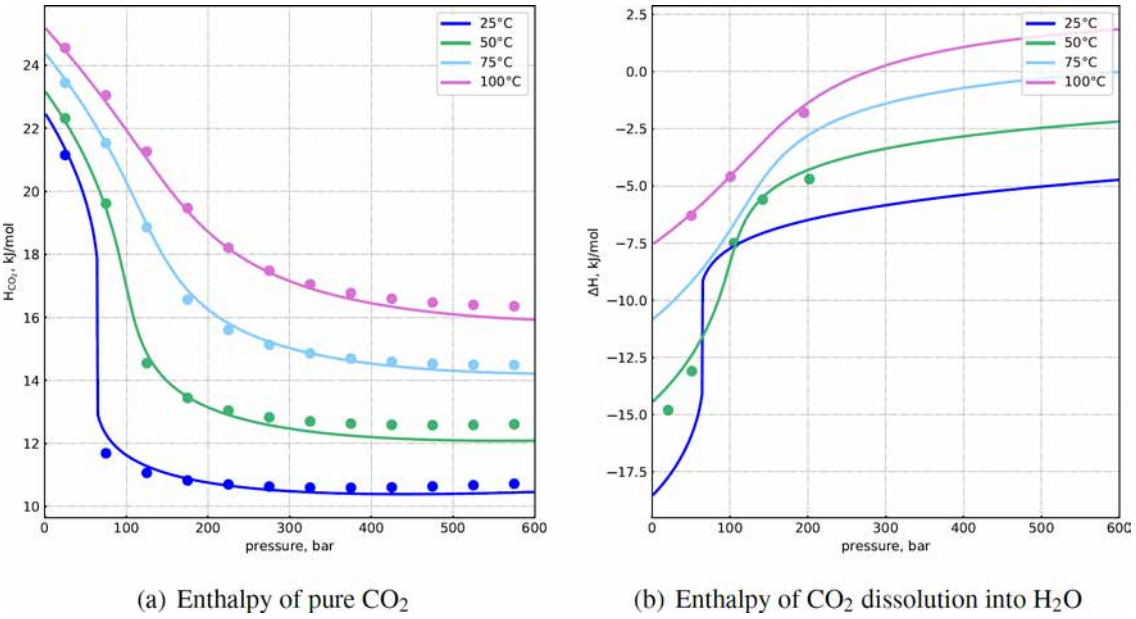

Figure 3—Thermal properties of a CO_2-brine system: (a) CO_2 enthalpy, data from (Lemmon et al., 2022), and (b) enthalpy of CO_2 dissolution in brine, data from (Koschel et al., 2006)

Modeling of core experiments relevant to CCUS

During the injection of CO_2 into the reservoir, the trailing front will be formed where CO_2 will vaporize the insitu brine. Brine dry-out can cause the precipitation of salt which is dissolved in the brine otherwise. If capillary backflow is present due to the heterogeneity of the reservoir, it can lead to a significant amount of precipitated salt which results in the blocking of the near-well porous region and increase the risk of rock damage due to the excessive pressure. Ott et al. (2015) have addressed this issue in a series of experimental and numerical studies for the heterogeneous sandstone cores. Recently, we extend this study and investigate the role of heterogeneity in salt precipitation (Van der Vleuten, 2022).

Following the experiments described by Van der Vleuten (2022), we illustrate the mechanism of salt precipitation from residual brine, which is vaporized by the dry CO_2 injection stream. In the setup presented here, we have used simplified values for the calculation of the reaction rate, as summarized in Table 1. The results of this setup are displayed in Figure 4. We emphasize the importance of accurate treatment of salinity in the activity model for the aqueous phase, as this affects the solubility of H_2O in the CO_2-rich phase. Presence of ions reduces the amount of vaporized H_2O, and thus controls the propagation of the vaporizing front.

Table 1—Input for determination of kinetic rates

Activity	Surface area A_s	Reaction constant c_k	Equilibrium constant K^{eq}
$x_{i,Aq}$ for ions, 1 for NaCl	1 m^2/m^3	0.1 kmol/m^2/day	100

Downloaded from http://onepetro.org/spersc/proceedings-pdf/23RSC/2-23RSC/D021S010R005/3095182/spe-212182-ms.pdf/1 by Bibliotheek TU Delft user on 18 April 2023

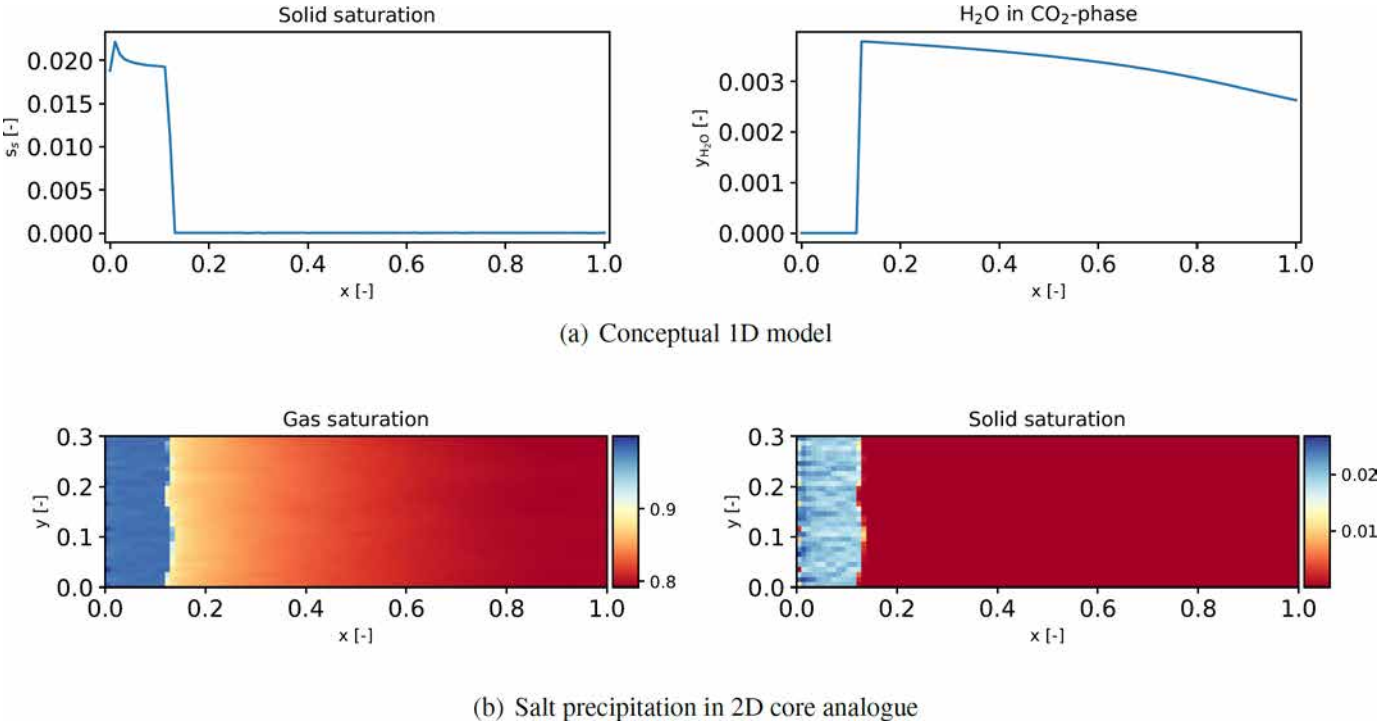

Figure 4—Simulation results of conceptual formation dry-out model in DARTS

The results are in qualitative agreement with our ongoing experimental study and we are currently in the process of quantitative validation of these simulations, with the inclusion of capillary pressure.

Modeling of large-scale experimental rig

The FluidFlower experimental rig comprises an engineered heterogeneous sand pack assembled within a thin (25mm) vertical Hele-Shaw cell, about 2.8m wide by 1.3m high (Nordbotten et al., 2022). The layered heterogeneous structure is filled using sands filtered into different grain sizes: the sand is placed in a layered fashion between the front glass panel and a sealed back panel with perforations for ports that can be used as injectors, producers, or pressure gauge locations. A sketch of the experimental rig with colored layers is shown in Figure 5a.

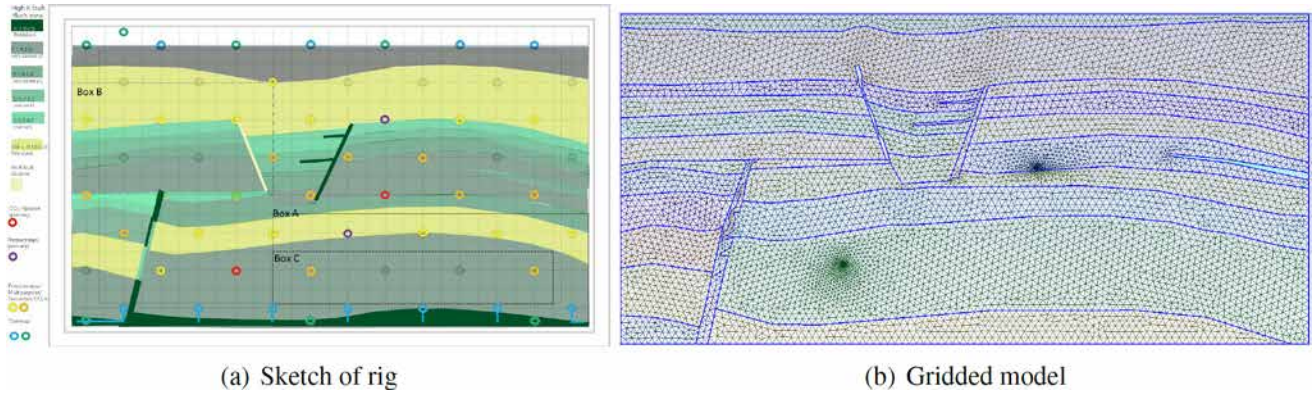

Figure 5—Sketch of the experimental rig geometry from FluidFlower benchmark description (Nordbotten et al., 2022) and gridded model

Experimentally, the sand facies have been sieved into groups labeled ESF, C, D, E, F, G, and there are 3 "fault" regions manufactured in the model. All measurements for porosity, permeability and capillary entry pressures of different types of sand have been performed in several independent sand-pack experiments.

Downloaded from http://onepetro.org/spersc/proceedings-pdf/23RSC/2-23RSC/D021S010R005/3095182/spe-212182-ms.pdf/1 by Bibliotheek TU Delft user on 18 April 2023

However, in this study, we will be using porosity, permeabilities, capillary pressure and injection rate scaled to idealized in-situ conditions of subsurface aquifers. The main parameters for each layer are specified in Table 2.

Table 2—Absolute permeabilities and porosities for modeling

Facies	Index *I*	Permeability [D]	Porosity	Entry pressure, bars
ESF	1	0.5	0.18	0.1
C	2	1	0.2	0.03
D	3	5	0.22	0.01
E	4	20	0.25	0.0
F	5	1	0.2	0.0
G	6	20	0.25	0.0
Fault1	7	20	0.25	0.0
Fault2	8	-	-	-
Fault3	9	20	0.25	0.0

The results of simulation are shown in Figure 6. The injection is performed in the first 5 hours and the monitoring last for the next 21 days. The results show the simulation results after 1 and 21 days. At first, the CO_2 is mostly trapped in the domes bounded by fine sand layers which serve as the structural trap due to the capillary entry pressure. With time, instabilities are formed at the interface between CO_2 and brine. The analytic estimation of onset time following Elenius et al. (2015) is around 1 day which is fully consistent with the simulation results. After 21 days, the dominating trapping mechanism is enhanced dissolution due to the gravitational instabilities.

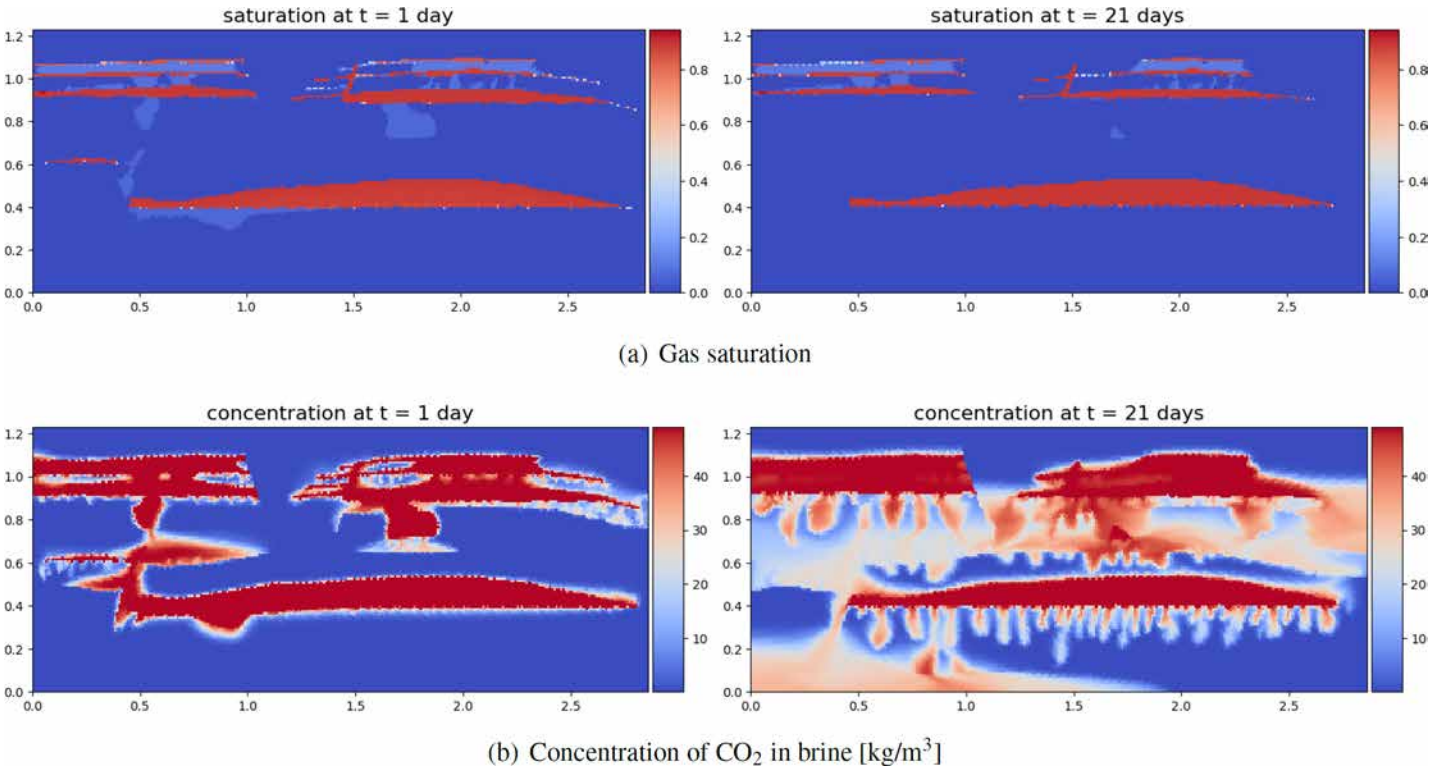

Figure 6—(a) Saturation and (b) concentration of CO_2 in brine at t = 1 day and t = 21 days

Downloaded from http://onepetro.org/spersc/proceedings-pdf/23RSC/2-23RSC/D021S010R005/3095182/spe-212182-ms.pdf/1 by Bibliotheek TU Delft user on 18 April 2023

Multi-scale simulation of enhanced CO_2 dissolution

In this subsection, we demonstrate our simulation framework in the 3D study of CO_2 injection and plume propagation. The main focus here is to capture the enhanced dissolution of CO_2 in a realistic heterogeneous reservoir based on the West Pernis field with a heterogeneous aquifer reservoir (Figure 7). We inject CO_2 by the well located at the bottom of the reservoir and investigate the propagation of CO_2 plume.

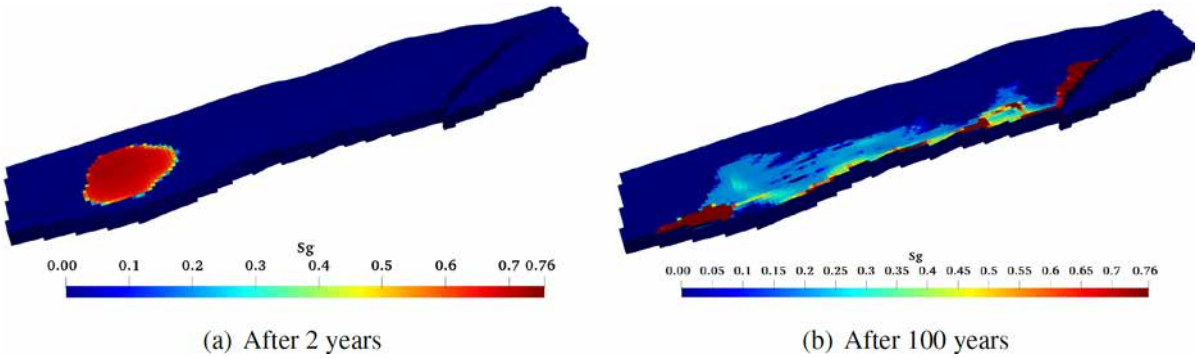

Figure 7—Simulation results at (a) the end of the injection period and (b) at the end of the simulation period.

The reservoir average pressure and temperature are 79 bar and 365 K, respectively. The CO_2 injection rate is 600×10^3 kg/day with a lower temperature of 315 K and with a maximum bottom-hole-pressure (BHP) constraint of 300 bar, above which the formation may be damaged. After two years of injection, the well was stopped and the migration of CO_2 plume is monitored. Figure 7 shows the saturation maps by the end of the injection period and by the end of simulation at 100 years.

However, this model significantly underestimates dissolution trapping of CO_2 since the grid resolution does not allow to capture the enhanced dissolution happening due to the instabilities of CO_2 current supported by the presence of capillary transition zone (Elenius et al., 2015). To accurately capture enhanced dissolution, we proposed a multiscale approach demonstrated at two representative elements: one is close to the injection well where the capillary transition zone is present; another element is in the region where the capillary effect can be neglected.

Figure 8 shows the location of these elements in the original model. Both elements are nine-block columns preserving the same geological properties as the original model. We mainly focus on the CO_2 migration in the central column, but the surrounding eight blocks are used to reflect the areal plume interaction. These two elements are refined with 120×120 gridblocks in the x-y plane (the horizontal size of blocks is 1 m), while the layering in the vertical direction is kept as in the original geological model with corresponding heterogeneity.

Downloaded from http://onepetro.org/spersc/proceedings-pdf/23RSC/2-23RSC/D021S010R005/3095182/spe-212182-ms.pdf/1 by Bibliotheek TU Delft user on 18 April 2023

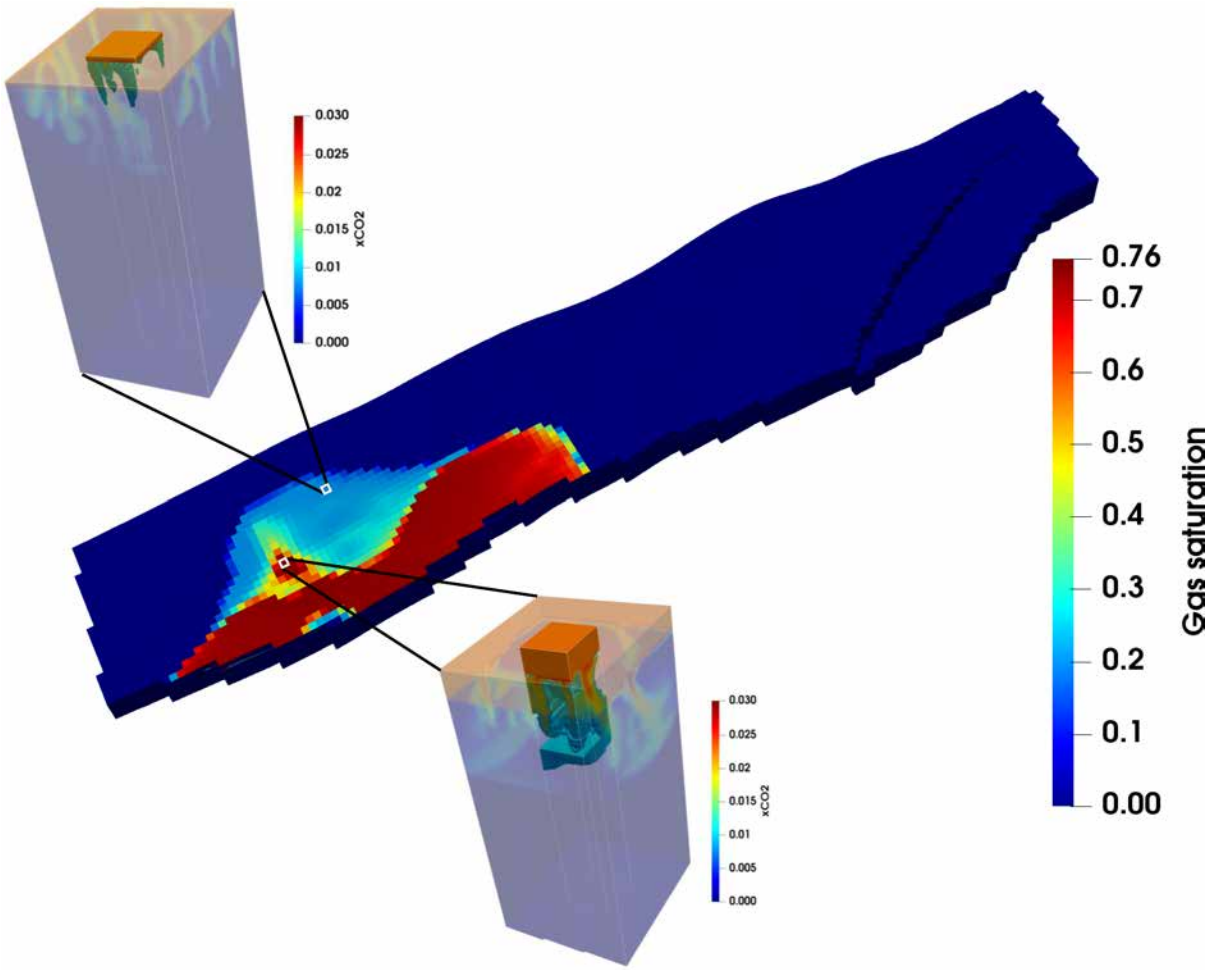

Figure 8—Location of two representative elements. The two elements are CO_2 mole fraction after 150 years in different elements, and a threshold ([0.01, 0.03]) is applied.

The subfigures in Figure 8 show CO_2 concentration after 150 years in both elements. After the onset of convection, CO_2 gradually dissolves into the underlying brine. With the consideration of the capillary effect in Element 1, CO_2 moves faster with a relatively higher concentration, which is consistent with the findings in Elenius et al. (2015). Due to the vertical heterogeneity, CO_2 fingers are not significantly scattered especially when they reach the lower-permeability layers. It starts to propagate laterally and fills in the domain progressively. The increase of average CO_2 concentration reduces the dissolution rate. Without the capillary transition zone in Element 2, the fingers are relatively thinner and move slower mainly due to the low permeability.

Figure 9 compares the mass transfer rate in both elements. The average mass transfer rate based on the analytic estimation is much higher than the rate predicted by the refined model for both Element 1 and 2. This happened due to the vertical heterogeneity in the realistic column model which limits the vertical propagation of CO_2, and it further reduces the dissolution rate. At the same time, in the coarse (field-scale) model, the dissolution is mostly driven by diffusion since the modeling resolution is not sufficient to represent enhanced dissolution. Thus, the dissolution rate decreases sharply with CO_2 propagation (Figure 9).

Downloaded from http://onepetro.org/spersc/proceedings-pdf/23RSC/2-23RSC/D021S010R005/3095182/spe-212182-ms.pdf/1 by Bibliotheek TU Delft user on 18 April 2023

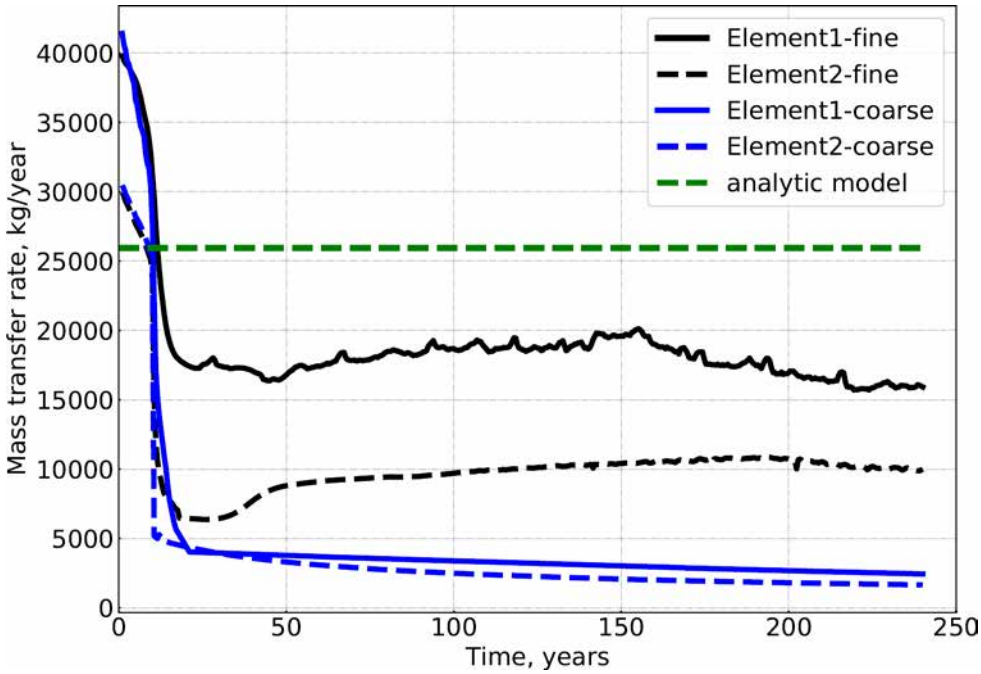

Figure 9—Variations of Mass transfer rate of each element with different mesh resolution. 'fine' stands for the results obtained from new mesh, and 'coarse' is the results from the original mesh.

This example indicates that CO_2 sequestration simulation in realistic reservoirs can either overestimate (using the semi-analytic technique) or underestimate (using direct numerical simulation at the reservoir scale) the enhanced dissolution rate. A high-resolution simulation is required to accurately predict the enhanced dissolution rate in the presence of realistic heterogeneity and proper variation of thermodynamic parameters. However, the computational cost of doing full-field simulations at appropriate resolution is very high. This study suggests an application of a multi-scale approach where enhanced dissolution can be corrected based on a localized highresolution simulation.

Conclusions

This work presents a unique uniform simulation framework for modeling of CCUS-related subsurface applications. In a modified version of the Delft Advanced Research Terra Simulator (DARTS), our formulation is extended to unify the mass and energy conservation equations for advective-diffusive compositional multiphase flow with chemical reactions for modeling various aspects of CO_2 sequestration problems. The OBL approach transforms the discretized nonlinear conservation equations into a quasilinear form according to state-dependent operators. Taking advantage of the flexibility of OBL, an advanced thermodynamic framework is implemented. Robust and efficient thermodynamic equilibrium calculations are performed using an accurate description of saline aqueous and CO_2-rich phases. Furthermore, kinetic mechanisms for salt precipitation are addressed. The thermodynamic package extends the ability for accurate modeling of thermo-hydro-chemical interactions of reservoir fluids and injection streams at different time and space scales. The framework is demonstrated to capture complex thermal-reactive phenomena such as Joule-Thomson cooling, mixing enthalpy and salt precipitation, and accurately describe the different trapping mechanisms involved in CCUS, residual, capillary and enhanced dissolution trapping.

Acknowledgements

We want to acknowledge the financial support of Michiel Wapperom by TotalEnergies. We thank Rouhi Fara- jzadeh for useful discussions about the salt precipitation problem.

Downloaded from http://onepetro.org/spersc/proceedings-pdf/23RSC/2-23RSC/D021S010R005/3095182/spe-212182-ms.pdf/1 by Bibliotheek TU Delft user on 18 April 2023

References

Ajayi, T., Awolayo, A., Gomes, J. S., Parra, H., and Hu, J. (2019). Large scale modeling and assessment of the feasibility of CO_2 storage onshore abu dhabi. *Energy*, **185**: 653–670.

Delshad, M., Kong, X., Tavakoli, R., Hosseini, S. A., and Wheeler, M. F. (2013). Modeling and simulation of carbon sequestration at cranfield incorporating new physical models. *International Journal of Greenhouse Gas Control*, **18**: 463–473.

Elenius, M., Voskov, D., and Tchelepi, H. (2015). Interactions between gravity currents and convective dissolution. *Advances in Water Resources*, **83**: 77–88.

Fan, Y., Durlofsky, L. J., and Tchelepi, H. A. (2012). A fully-coupled flow-reactive-transport formulation based on element conservation, with application to CO_2 storage simulations. *Advances in Water Resources*, **42**: 47–61.

Kala, K. and Voskov, D. V. (2020). Element balance formulation in reactive compositional flow and transport with parameterization technique. *Computational Geosciences*, **24**: 609–624.

Khait, M. and Voskov, D. V. (2018a). Adaptive parameterization for solving of thermal/compositional nonlinear flow and transport with buoyancy. *SPE Journal*, **23**(02): 522–534.

Khait, M. and Voskov, D. V. (2018b). Operator-based linearization for efficient modeling of geothermal processes. *Geothermics*, **74**: 7–18.

Kim, K.-Y., Han, W. S., Oh, J., Kim, T., and Kim, J.-C. (2011). Characteristics of salt-precipitation and the associated pressure build-up during CO_2 storage in saline aquifers. *Transport in Porous Media*, 92.

Koschel, D., Coxam, J.-Y., Rodier, L., and Majer, V. (2006). Enthalpy and solubility data of CO_2 in water and NaCl (aq) at conditions of interest for geological sequestration. *Fluid Phase Equilibria*, **247**: 107–120.

Lemmon, E. W., Bell, I. H., Huber, M. L., and McLinden, M. O. (2022). Thermophysical Properties of Fluid Systems. *National Institute of Standards and Technology, Gaithersburg (MD)*.

Lyu, X., Khait, M., and Voskov, D. (2021). Operator-based linearization approach for modelling of multiphase flow with buoyancy and capillarity. *SPE Journal*, **26**(04): 1858–1875.

Michelsen, M. L. and Mollerup, J. M. (2007). Thermodynamic Models: Fundamentals & Computational Aspects. *Tie-Line Publications*.

Nichita, D. and Leibovici, C. (2013). A rapid and robust method for solving the rachford-rice equation using convex transformations. *Fluid Phase Equilibria*, **353**: 38–49.

Nordbotten, J. M., Fernø, M., Flemisch, B., Juanes, R., and Jørgensen, M. (2022). *Final Benchmark Description: FluidFlower International Benchmark Study*.

Oldenburg, C. M. (2007). Joule-thomson cooling due to CO_2 injection into natural gas reservoirs. *Energy Conversion and Management*, **48**(6): 1808 – 1815.

Ott, H., Roels, S., and de Kloe, K. (2015). Salt precipitation due to supercritical gas injection: I. capillary-driven flow in unimodal sandstone. *International Journal of Greenhouse Gas Control*, **43**: 247–255.

Ott, H., Snippe, J., and de Kloe, K. (2021). Salt precipitation due to supercritical gas injection: Ii. capillary transport in multi porosity rocks. *International Journal of Greenhouse Gas Control*, **105**: 103233.

Peng, D.-Y. and Robinson, D. B. (1976). A new two-constant equation of state. *Ind. Eng. Chem., Fundam.*, **15**(1): 59–64.

Petitfrere, M., Nichita, D., Voskov, D., Zaydullin, R., and Bogdanov, I. (2020). Full-eos based thermal multiphase compositional simulation of CO_2 and steam injection processes. *Journal of Petroleum Science and Engineering*, **192**(107241).

Pruess, K. and Müller, N. (2009). Formation dry-out from CO_2 injection into saline aquifers: 1. effects of solids precipitation and their mitigation. *Water Resources Research*, **45**: W03402.

Pruess, K. and Nordbotten, J. (2011). Numerical simulation studies of the long-term evolution of a CO_2 plume in a saline aquifer with a sloping caprock. *Transport in Porous Media*, **90**: 135–151.

Ringrose, P. (2020). How to Store CO_2 Underground: Insights from early-mover CCS Projects. *SpringerBriefs in Earth Sciences*.

Spycher, N., Pruess, K., and Ennis-King, J. (2003). CO_2-H_2O mixtures in the geological sequestration of CO_2. i. assessment and calculation of mutual solubilities from 12 to 100°c and up to 600 bar. *Geochimica et Cosmochimica Acta*, **67**(16): 3015–3031.

Van der Vleuten, R. (2022). Impact of reservoir heterogeneity on dry-out effect during CO_2 injection. Master's thesis, TU Delft, Geoscience and Engineering.

Voskov, D. (submitted in 2016). Coarsening of physical representation in multiphase compositional model. *JCP*.

Whitson, C. H. and Michelsen, M. L. (1989). The negative flash. *Fluid Phase Equilibria*, **53**: 51–71.

Ziabakhsh-Ganji, Z. and Kooi, H. (2012). An equation of state for thermodynamic equilibrium of gas mixtures and brines to allow simulation of the effects of impurities in subsurface CO_2 storage. *International Journal of Greenhouse Gas Control*, **11S**: S21–S34.

Downloaded from http://onepetro.org/spersc/proceedings-pdf/23RSC/2-23RSC/D021S010R005/3095182/spe-212182-ms.pdf/1 by Bibliotheek TU Delft user on 18 April 2023